The Astrophysical Journal, 903:42 (18pp), 2020 November 1 https://doi.org/10.3847/1538-4357/abbb95
© 2020. The American Astronomical Society. All rights reserved.

A Search for In Situ Field OB Star Formation in the Small Magellanic Cloud

Irene Vargas-Salazar[1], M. S. Oey[1], Jesse R. Barnes[1,4], Xinyi Chen[1,5], N. Castro[2], Kaitlin M. Kratter[3], and Timothy A. Faerber[1,6]
[1] University of Michigan, 1085 S University Ave., Ann Arbor, MI 48109, USA; ivargasa@umich.edu
[2] Leibniz-Institut für Astrophysik An der Sternwarte, 16 D-14482, Potsdam, Germany
[3] University of Arizona, Tucson, AZ 85721, USA
Received 2020 July 27; revised 2020 September 21; accepted 2020 September 23; published 2020 October 30

Abstract

Whether any OB stars form in isolation is a question central to theories of massive star formation. To address this, we search for tiny, sparse clusters around 210 field OB stars in the Small Magellanic Cloud (SMC) from the Runaways and Isolated O-Type Star Spectroscopic Survey of the SMC (RIOTS4), using friends-of-friends and nearest neighbors algorithms. We also stack the target fields to evaluate the presence of an aggregate density enhancement. Using several statistical tests, we compare these observations with three random-field data sets, and we also compare the known runaways to nonrunaways. We find that the local environments of nonrunaways show higher aggregate central densities than for runaways, implying the presence of some "tips of icebergs" (TIB) clusters. We find that the frequency of these tiny clusters is low, ∼4%–5% of our sample. This fraction is much lower than some previous estimates, but is consistent with field OB stars being almost entirely runaway and walkaway stars. The lack of TIB clusters implies that such objects either evaporate on short timescales or do not form, implying a higher cluster lower-mass limit and consistent with a relationship between maximum stellar mass ($m_{\rm max}$) and the mass of the cluster ($M_{\rm cl}$). On the other hand, we also cannot rule out that some OB stars may form in highly isolated conditions. Our results set strong constraints on the formation of massive stars in relative isolation.

Unified Astronomy Thesaurus concepts: Massive stars (732); Field stars (2103); Small Magellanic Cloud (1468); Star clusters (1567); Open star clusters (1160); Star formation (1569); Runaway stars (1417); Galaxy stellar content (621); Initial mass function (796); Multiple star evolution (2153); OB associations (1140); OB stars (1141)

1. Introduction

Roberts (1957) first examined the question of whether all massive stars form in clusters or whether a significant number might form in isolation as field stars. Based on the limited data of that era, he concluded that OB stars rarely, if ever, form in the field. Additionally, there is evidence to suggest that star formation occurs in unbound associations of OB stars (Griffiths et al. 2018; Ward et al. 2020). However, while it is widely accepted that most massive stars form in clusters or associations (e.g., Elmegreen 1985; Lada & Lada 2003; Zinnecker & Yorke 2007), it is well known that a significant population of massive stars is also found in sparse field environments. The reported frequency of field OB stars varies, depending on how the "field" is defined, but it is on the order of 20%–30% (e.g., Gies 1987; Oey et al. 2004).

In spite of their significant numbers, the nature and origin of the field massive stars have been unclear. Previous investigations on the cluster mass function imply that many, if not most, field OB stars formed in situ (e.g., Oey et al. 2004; Lamb et al. 2010). On the other hand, large populations of runaway OB stars are also known to exist and may dominate the field population (e.g., de Wit et al. 2005; Oey et al. 2018; Renzo et al. 2019).

1.1. In Situ Field OB Star Formation

The degree to which massive stars can form in isolation provides an important discriminant between the two dominant theories of massive star formation: competitive accretion and core accretion. The competitive accretion model theorizes that cores accrete matter from a shared reservoir of gas (Zinnecker 1982). The core with the highest mass accretes the most matter because of its size and location at the center of the subcluster (Bonnell et al. 2001), while lower-mass cores accrete the remaining gas. Thus, this model requires that low-mass stars must form in the presence of massive stars, and vice versa (Bonnell et al. 2004), yielding a spectrum of stellar masses (e.g., Zinnecker 1982; Bonnell et al. 2001). This stipulation implies a relationship between the mass of the most massive star formed in the cluster $m_{\rm max}$ and the total mass of the cluster $M_{\rm cl}$, by $m_{\rm max} \propto M_{\rm cl}^{2/3}$ (Bonnell et al. 2004).

In contrast, the core accretion model allows for occasional formation of isolated massive stars (Li et al. 2003; Krumholz et al. 2009). The model is a scaled-up version of low-mass star formation. It suggests that cores do not compete to accrete gas, and instead the amount of gas they accrete depends on the masses of the cores themselves before collapse (Shu et al. 1987). Clouds maintain their mass because fragmentation is prevented by heating from the accretion process (Krumholz & McKee 2008). Monolithic collapse could then finally happen for sufficiently dense clouds with high column densities (at least 1 g cm^{-2}), forming massive stars. Thus, if OB stars are able to form in situ in the field, this would provide substantial evidence favoring the core accretion model, whereas competitive accretion requires all OB stars to form in clusters.

Oey et al. (2004) found that OB clusters and the H II region luminosity function (e.g., Oey & Clarke 1998; Oey et al. 2003) follow a power-law distribution $\sim N_*^{-2}$ for the number of OB stars N_* per cluster. This power law extends to the extreme value of $N_* = 1$, implying that OB stars with no other nearby massive stars appear as field stars, simply by populating the

[4] Present address: Private.
[5] Present address: Yale University, New Haven, CT 06520, USA.
[6] Present address: Department of Physics and Astronomy, Uppsala University, Box 516, SE-751 20 Uppsala, Sweden.

low end of the cluster mass function. These individual field OB stars may simply be the "tip of the iceberg" (TIB) on tiny, sparse clusters at the low-mass extreme that are difficult to detect. Lamb et al. (2010) provide evidence for the existence of such sparse clusters, or minimal O star groups, associated with field OB stars in the Small Magellanic Cloud (SMC). With observational data from the Hubble Space Telescope on eight SMC field OB stars, they find that three out of the eight are in sparse clusters with $\leqslant 10$ companion stars, each having masses of 1–4$M_{\odot}$.

Additionally, the existence of these sparse clusters is consistent with the stochastic nature of the cluster mass function and the stellar initial mass function (IMF). Monte Carlo simulations show that tiny clusters with OB stars can occur if clusters are built stochastically by randomly sampling stars from a universal IMF, which implies that the maximum stellar mass in a cluster is independent of cluster mass (Parker & Goodwin 2007; Lamb et al. 2010). However, Monte Carlo simulations by Weidner & Kroupa (2006) tested various methods of populating clusters including a completely stochastic sampling. They found that clusters populated through random sampling do not fit observations of young clusters as well as a cluster populated through sorted sampling, in which stellar masses are sorted in ascending order and their sum is constrained to be the cluster mass. This would imply that clusters form in an organized fashion and is consistent with the relation $m_{\rm max} \propto M_{\rm cl}^{2/3}$.

An important test for star formation and cluster models is thus the existence of truly isolated, in situ OB star formation. We note that this is true whether or not "isolated" OB stars are binaries, since most binaries form from a single star-forming core. While it is currently almost impossible to determine whether any OB stars form in true isolation, some tantalizing observations exist. In the SMC, Oey et al. (2013) present a sample of 14 field OB stars that are strong candidates for in situ formation. These objects are found in the center of circular H II regions, showing no bow shocks, implying supersonic motion, and having radial velocities matching those of the local HI components. Five of these targets are extremely isolated. Also in the SMC, observations by Selier et al. (2011) show that the compact H II region N33 is consistent with this object being a case of isolated massive-star formation. In the 30 Doradus region of the LMC, Bressert et al. (2012) identified 15 O stars as candidates for isolated formation. These stars are not in binary systems and show no evidence of clustering. Additionally, Oskinova et al. (2013) suggest that one of the most massive stars in the Milky Way, WR102ka, may have been born in isolation. It is not a runaway because it shows a circumstellar nebula with no bow shock, and there is no evidence of an associated star cluster. de Wit et al. (2004) found that $4\% \pm 2\%$ (4–11 out of 193) of the Galactic O star population either cannot be traced to OB associations or have nonrunaway space velocities.

1.2. Runaway and Walkaway OB Stars

OB stars that are ejected from clusters could be runaway stars ($>30\,{\rm km\,s^{-1}}$) or walkaways, slower stars that are unbound but below the runaway threshold velocity. These are known to comprise a significant fraction of the field OB population (e.g., Blaauw 1961). Over the course of their lifetimes, these stars move far beyond their original birthplaces, and so by definition they are distinct from stars in clusters. There are two mechanisms for producing runaways and walkaways: dynamical ejection (Poveda et al. 1967) and binary supernova ejection (Blaauw 1961). The dynamical mechanism ejects stars primarily from unstable three- or four-body systems (Leonard & Duncan 1990) and is prevalent in dense cluster cores. In the binary supernova scenario, the primary star of a binary system explodes as a supernova, which ejects the secondary star by a slingshot release that may be combined with a supernova "kick."

The frequency of runaway OB stars is not well established, but it is generally believed to be large. Some estimates suggest that it is on the order of 50% of the field OB star population (e.g., Gies & Bolton 1986; de Wit et al. 2005), while others suggest that almost all field OB stars are runaways (e.g., Gies 1987; Gvaramadze et al. 2012). Recent work from our group using Gaia DR2 proper motions is consistent with runaways strongly dominating the field OB population in the SMC (Oey et al. 2018; Dorigo Jones et al. 2020).

1.3. Remnants of Evaporated Clusters

Another way to generate field OB stars is a hybrid between in situ star formation and dynamical effects. The loss of stars from small clusters may result in some of these being much smaller than when they formed, and if an OB star is present, it would be observed as a TIB star, as described in Section 1.1. In the most extreme case, the OB star could be completely abandoned by its cohorts, although studies are needed to determine the likelihood of this scenario. Many clusters, especially at low mass, become unbound by gas expulsion and feedback not long after the stars form, a phenomenon dubbed "infant mortality" or "infant weight loss" (e.g., Lada & Lada 2003; Goodwin & Bastian 2006). However, Farias et al. (2018) suggest that gas expulsion may be more difficult than previously believed. Alternatively, Ward et al. (2020) find that the formation of smaller, unbound associations with OB stars may be relatively commonplace, even in lower density environments, thus supporting scenarios where massive stars are not all formed in bound clusters. There is evidence of this in the Cyg OB2 association, which has a high frequency of wide binaries that would be disrupted through dynamical encounters in clusters (Griffiths et al. 2018), but are possible if they form in unbound associations.

2. A Search for Field OB Star Formation

To understand the contribution, if any, of in situ OB star formation to the field massive-star population, we search for small clusters associated with field OB stars in the SMC to establish and quantify their existence. The SMC offers a complete sample of field OB stars in an external galaxy and is located at a well-determined distance of 60 kpc (Harries et al. 2003). We employ two different cluster-finding algorithms, friends of friends (FOF; Battinelli 1991) and nearest neighbors (NN; Schmeja 2011), and we also examine the stacked fields around the target OB stars for an aggregate density enhancement.

We note that OB stars have a high multiplicity fraction. This implies that TIB stars in small clusters also may be binaries or multiples, which are difficult to discern. Studies have shown that field massive stars also may have significant binarity, from about half the binary frequency of those in clusters (Stone 1981; Gies 1987) to frequencies on the order of those in clusters (Mason et al. 2009; Lamb et al. 2016).

To carry out our analysis, we use the Runaways and Isolated O-Type Star Spectroscopic Survey of the SMC (RIOTS4; Lamb et al. 2016), which identifies a uniform, statistically

complete sample of field massive stars in the SMC. RIOTS4 represents the field-star subset of OB star candidates that were photometrically identified by Oey et al. (2004) from the Massey (2002) survey of the SMC, which covers the star-forming expanse of the galaxy. Field stars were differentiated from cluster stars by identifying stars that are at least 28 pc away from any other OB candidates in the analysis of Oey et al. (2004). The RIOTS4 field stars are all spectroscopically confirmed OB stars (Lamb et al. 2016), and they represent ∼28% of the total SMC OB population (Oey et al. 2004). Lamb et al. (2016) find a binary frequency of $\gtrsim$60% in this sample.

To search for small, sparse clusters associated with the field OB stars, we require deep stellar imaging of their fields. The Optical Gravitational Lensing Experiment (OGLE-III; Udalski et al. 2008) has accumulated *I*-band photometry on the SMC for many years. OGLE-III uses the 1.3 m Warsaw Telescope at Las Campanas. Each CCD image is 35 × 35 arcmin^2 with a scale of 0.″26 pixel^{-1}.

To carry out our cluster-finding algorithms, we require high-quality astrometry of all of the stars near our target OB stars. Given the crowded fields in the SMC Bar region, we therefore performed point-spread function (PSF)-fitting photometry and astrometry on 1000 × 1000 px^2 (76 × 76 pc^2) subframes centered on the target stars. We used the DAOphot software in IRAF[7] applied to the OGLE-III *I*-band images. The image PSFs are generally on the order of 3.0 pixels, or 0.23 pc FWHM with variation on the order of 10%. Within a 200 pixel (15 pc) radius of the target, each field was carefully vetted with both automatic and manual identification of the stellar objects, to optimize the sample completeness. We then calibrated the photometry for the entire field using the published OGLE-III photometry (Udalski et al. 2008). Our photometric errors indicate that the data have excellent completeness for $I < 19.0$, and we applied this cutoff to our data set.

Our final sample comprises 210 field OB stars. There are fewer stars in our sample than in the original RIOTS4 survey for several reasons. First, the OGLE-III survey excludes the easternmost region of the SMC Wing. Second, targets that are <200 pixels from the edge of the OGLE-III CCD frames were discarded, since the cluster-finding algorithms rely on the complete spatial distribution of stars near the target. In addition, there are targets for which we were unable to carry out the astrometry and photometry because of technical issues related to field placement within the frame, such as the presence of an extremely bright foreground star within the field, and spatial distortions near the detector edge. Finally, six stars (M2002-SMC 11802, 38893, 42654, 46022, 62981, and 67029; Massey 2002) in the RIOTS4 sample were inadvertently included even though they did not meet the criterion of being 28 pc from another OB candidate; these were also deleted from our sample.

2.1. Friends of Friends

The FOF cluster-finding method uses a methodology similar to a minimum spanning tree algorithm. It identifies associated stars, or "friends," as those that are located within a given clustering length (l_c) of another member.

[7] IRAF was distributed by the National Optical Astronomy Observatory, which was managed by the Association of Universities for Research in Astronomy (AURA) under a cooperative agreement with the National Science Foundation.

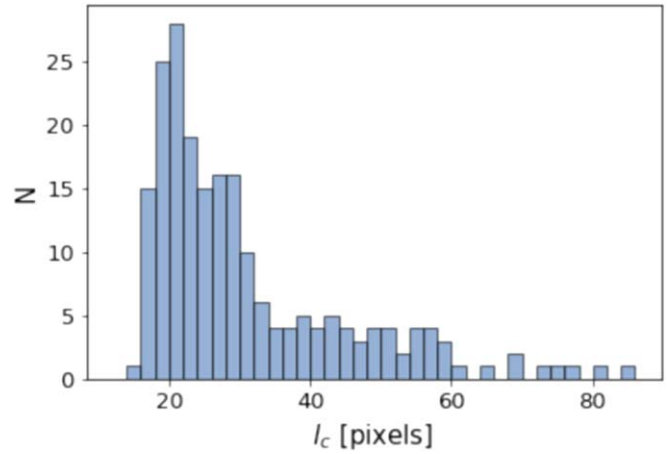

Figure 1. Distribution of clustering length l_c for stars having $I < 19.0$ in our target fields. The lower stellar density in the Wing generates a long tail in the distribution to values much greater than those for bound stars in clusters. Therefore, a maximum value of $l_c = 39$ px is adopted for fields with $l_c > 50$ px.

We use the FOF algorithm in this manner to search for faint companion stars in the OGLE-III images with $I < 19.0$ ($M_I = 0.11$, corresponding roughly to an A1 star), which might correspond to small clusters, of which our target OB stars are the TIBs. The FOF clustering length, l_c, is the value characteristic of the background stellar density. Since our target OB stars are in locations of varying background density, we define l_c specific to each field. To do this, we calculate the number of clusters found as a function of different clustering lengths in a given field. The value that yields the maximum number of clusters is adopted as the l_c of the field (Battinelli 1991). Our distribution of our final l_c for our target fields is shown in Figure 1.

The Wing of the SMC has a much lower stellar density than the Bar, generating a long tail in the l_c distribution (Figure 1), to values much greater than what are likely to include bound stars in tiny clusters. We therefore adopt a maximum fixed l_c of 39 pixels (3.0 pc), which is 1σ above the median value, for any l_c above 50 pixels. This is on the order of the core radii for small clusters (Lada & Lada 2003).

An inherent weakness in the FOF algorithm is that it has the tendency to associate stars in a filamentary structure that are physically unrelated. Although some clusters show real filamentary structure, the fact that this algorithm identifies such formations in artificial data demonstrates that it could overestimate N_* (Schmeja 2011). An example of this type of structure is shown in Figure 2.

We then apply the FOF algorithm, using the target OB stars as the origin for the algorithm. We evaluate the results using two criteria (Campana et al. 2008; Schmeja 2011), one based on the number of stars (N_*) that are found to be associated; and another based on the *M*-value, which is a parameter that also takes into account the separation of the identified associated stars (see below). For both of these tests, a larger value indicates a higher probability that the associated stars correspond to a real cluster.

However, some clusters do have a filamentary structure, and we cannot reliably distinguish cases that are real from those that are not. Therefore, we generate three realizations of random-field data sets for each of our targets to serve as controls. The random fields have the same size (1000 × 1000 px^2) and the same number of

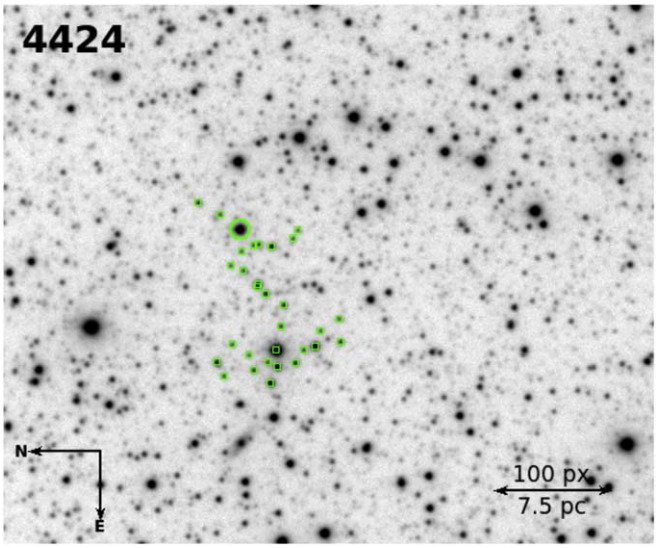

Figure 2. Example of a filamentary string-like structure that occurs with FOF. Target 4424 is shown by the green circle.

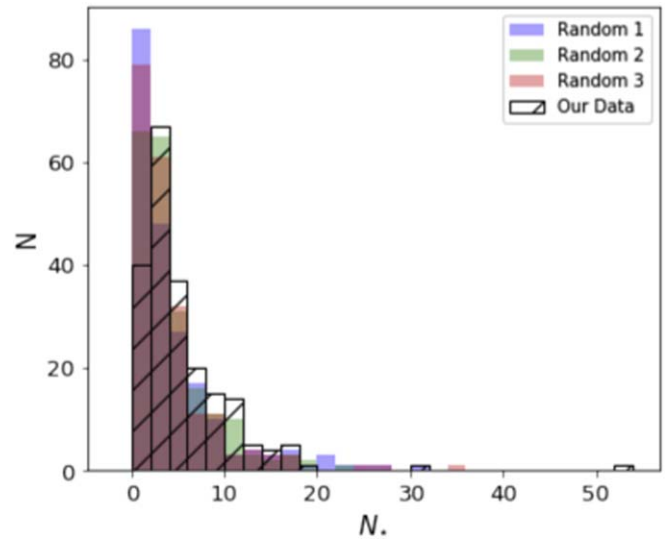

Figure 3. Distribution of N_*, the number of stars associated by FOF for stars with $I < 19.0$. Our observed data set is plotted in black, and the random fields are colored. The Wilcoxon test indicates that our observed data and random fields are distinct, while our Rosenbaum test results reveal ambiguous results.

stars as the observed field for our targets, but with the stars randomly placed. This also allows us to evaluate the potential effects of random Poisson noise on the observed data.

Our N_* distribution, as well as those from the random fields, is shown in Figure 3. We see that the observed distribution differs from the random fields at small N_* values, but they are otherwise remarkably similar.

We use the Wilcoxon signed rank test for matched pairs to evaluate whether the observed and randomized distributions are statistically indistinguishable. This test is appropriate for two nonparametric data sets that are not independent, and is calculated from the difference between the pairs of data points for each field, the observed versus random field. The results are shown in Table 1. We adopt the conventional critical threshold of $p < 0.05$ for rejecting the null hypothesis that the two distributions originate from the same parent distribution. Comparing the N_* distributions, we obtain p-values that strongly indicate that the observed data set differs from the randomized ones, indicating the potential presence of some TIB clusters.

We might expect that the tails of the distributions should be sensitive to the presence of TIB clusters, which would have higher positive N_* values and would skew both the median and the tail to higher values. The Rosenbaum test (Rosenbaum 1965) is optimized to evaluate the significance of differences in the tails of two distributions, by counting the number of data points between the highest values of the two samples and quantifying the significance of the difference. Using this test, we do not obtain a significant difference in spread, although the higher value does belong to our observed data set in each case, when compared to the random data sets. The results are given in Table 1 and show p-values higher than our threshold of 0.05, indicating that the tails of the observed data set versus the randomized ones do not differ statistically.

The second criterion we use to search for cluster candidates uses the M-values (Campana et al. 2008; Schmeja 2011), where

$$M = \frac{l_{c,\mathrm{SMC}}}{l_{c,\mathrm{field}}} N_*. \tag{1}$$

This takes the ratio of the average clustering length for all of the SMC fields ($l_{c,\mathrm{SMC}}$) and the clustering length of a given field ($l_{c,\mathrm{field}}$) and multiplies it by the number of stars associated by FOF for that particular field. Therefore, this test not only uses N_* but also takes into account the separation between these stars. A higher M-value corresponds to a larger number of stars that are closely spaced. The distribution of M-values is shown in Figure 4 for our observed data set and the random fields.

We again find that the M-value distributions for our observed data and the random fields have different statistical test results. The Wilcoxon test p-values indicate that the observed and random data sets are statistically distinct, while the Rosenbaum test results do not show a significant difference in spread. It is possible that the Wilcoxon signal results from the presence of some tiny clusters that are too small to affect the Rosenbaum tests. On the other hand, this outcome could also be due to the background stars having positions that are not purely random. This is further discussed in Section 3.

2.2. Nearest Neighbors

NN is an algorithm that measures the stellar density (Σ_j) associated with a given target star. This is calculated by counting the number of stars enclosed within the radius to its jth nearest neighbor in 2D as shown in Equation (2) (e.g., Schmeja 2011):

$$\Sigma_j = \frac{j-1}{S_j}, \tag{2}$$

where j is the jth nearest neighbor and S_j is the area defined by the radius to the jth nearest neighbor.

We compare the resulting stellar density to the background density. Since the background density varies greatly across the SMC, we perform background density calculations for each target individually. The average background density (Σ_{bg}) is calculated from the total number of stars in the field N_t, the total number of stars N_j within S_j, and the area outside S_j, so as to not include the area within a potential cluster, as shown in

Table 1
Statistical Test Results

Algorithm	Statistical Test	Data Set	p-Values[a]
FOF N_*	Wilcoxon	Full Data vs. Random 1	**0.001**
		Full Data vs. Random 2	**0.006**
		Full Data vs. Random 3	**2.2e-5**
		Runaways vs. Random 1	**0.010**
		Runaways vs. Random 2	**0.034**
		Runaways vs. Random 3	**0.020**
		Nonrunaways vs. Random 1	**0.003**
		Nonrunaways vs. Random 2	**0.044**
		Nonrunaways vs. Random 3	**0.002**
	Anderson–Darling	Runaways vs. Nonrunaways	0.71
	Kolmogorov–Smirnov	Runaways vs. Nonrunaways	0.96
	Rosenbaum	Full Data vs. Random 1	0.25
		Full Data vs. Random 2	0.25
		Full Data vs. Random 3	0.5
		Runaways vs. Random 1	0.5
		Runaways vs. Random 2	0.5
		Runaways vs. Random 3	0.5
		Nonrunaways vs. Random 1	0.5
		Nonrunaways vs. Random 2	0.5
		Nonrunaways vs. Random 3	0.5
FOF M-Test	Wilcoxon	Full Data vs. Random 1	**0.001**
		Full Data vs. Random 2	**0.010**
		Full Data vs. Random 3	**0.001**
		Runaways vs. Random 1	**0.006**
		Runaways vs. Random 2	**0.015**
		Runaways vs. Random 3	**0.003**
		Nonrunaways vs. Random 1	0.058
		Nonrunaways vs. Random 2	0.14
		Nonrunaways vs. Random 3	**0.001**
	Anderson–Darling	Runaways vs. Nonrunaways	0.44
	Kolmogorov–Smirnov	Runaways vs. Nonrunaways	0.51
	Rosenbaum	Full Data vs. Random 1	0.5
		Full Data vs. Random 2	0.25
		Full Data vs. Random 3	0.5
		Runaways vs. Random 1	0.5
		Runaways vs. Random 2	0.5
		Runaways vs. Random 3	0.5
		Nonrunaways vs. Random 1	0.5
		Nonrunaways vs. Random 2	0.5
		Nonrunaways vs. Random 3	−0.5
NN Average	Wilcoxon	Full Data vs. Random 1	**1.4e-5**
		Full Data vs. Random 2	**2.3e-5**
		Full Data vs. Random 3	**0.001**
		Runaways vs. Random 1	**0.028**
		Runaways vs. Random 2	**0.016**
		Runaways vs. Random 3	**0.020**
		Nonrunaways vs. Random 1	**5.8e-5**
		Nonrunaways vs. Random 2	**2.6e-4**
		Nonrunaways vs. Random 3	**0.013**
	Anderson–Darling	Runaways vs. Nonrunaways	0.067
	Kolmogorov–Smirnov	Runaways vs. Nonrunaways	**0.022**
	Rosenbaum	Full Data vs. Random 1	0.25
		Full Data vs. Random 2	**0.016**
		Full Data vs. Random 3	0.5
		Runaways vs. Random 1	-0.25
		Runaways vs. Random 2	0.5
		Runaways vs. Random 3	−0.5
		Nonrunaways vs. Random 1	**0.031**
		Nonrunaways vs. Random 2	**0.0078**
		Nonrunaways vs. Random 3	0.5
NN Median	Wilcoxon	Full Data vs. Random 1	**1e-5**
		Full Data vs. Random 2	**4.7e-5**
		Full Data vs. Random 3	**0.001**

Table 1
(Continued)

Algorithm	Statistical Test	Data Set	p-Values[a]
		Runaways vs. Random 1	**0.020**
		Runaways vs. Random 2	**0.019**
		Runaways vs. Random 3	**0.023**
		Nonrunaways vs. Random 1	**7.5e-5**
		Nonrunaways vs. Random 2	**0.001**
		Nonrunaways vs. Random 3	**0.018**
	Anderson–Darling	Runaways vs. Nonrunaways	0.090
	Kolmogorov–Smirnov	Runaways vs. Nonrunaways	**0.035**
	Rosenbaum	Full Data vs. Random 1	0.25
		Full Data vs. Random 2	**0.016**
		Full Data vs. Random 3	0.5
		Runaways vs. Random 1	−0.25
		Runaways vs. Random 2	0.5
		Runaways vs. Random 3	−0.5
		Nonrunaways vs. Random 1	**0.031**
		Nonrunaways vs. Random 2	**0.0078**
		Nonrunaways vs. Random 3	0.5

Notes.
[a] A higher p-value indicates a higher probability for the null hypothesis that the two distributions originate from the same parent distribution. The negative p-values indicate comparisons for which the cluster-finding test favors the random data set. The bold p-values indicate statistically significant differences ($p < 0.05$).

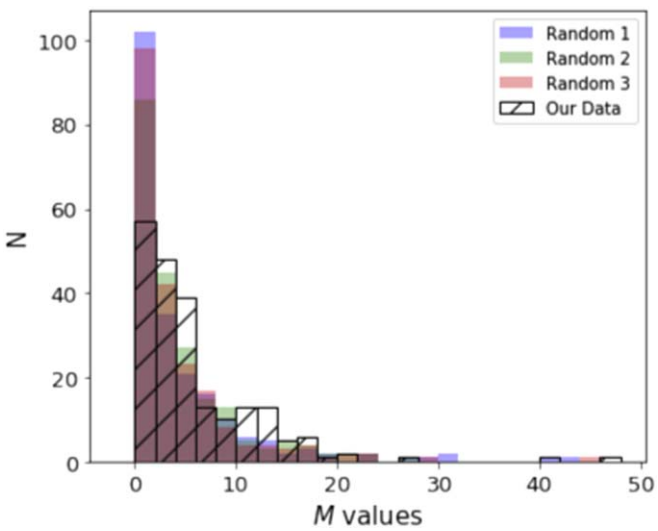

Figure 4. Distributions of M-values for FOF applied to stars with $I < 19.0$. Our observed data set is plotted in black, while the random fields are colored. These results are similar to our N_* results.

Equation (3):

$$\Sigma_{\rm bg} = \frac{N_t - N_j}{S_t - S_j}, \tag{3}$$

where S_t is the total area of the field (1000×1000 px^2). The Poisson error of $\Sigma_{\rm bg}$ is therefore

$$\sigma_{\rm bg} = \Sigma_{\rm bg} \times N_{{\rm bg},j}^{-1/2}, \tag{4}$$

where $N_{{\rm bg},j} = \Sigma_{\rm bg} \times S_j$ is the number of background stars expected in area S_j. We caution that some of our fields may occasionally include external clusters or overdensities in the background, which would overestimate the background.

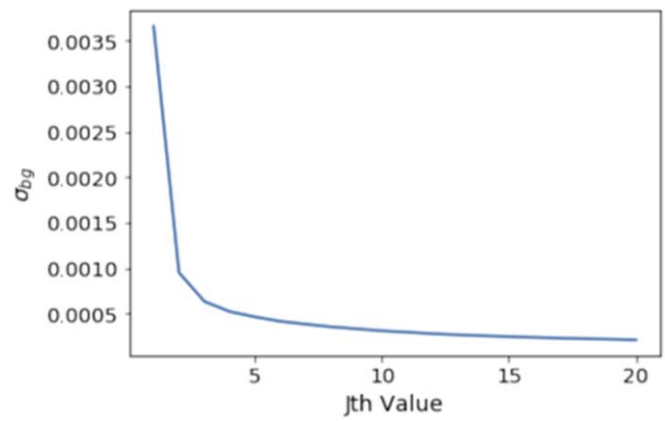

Figure 5. Average $\sigma_{\rm bg}$ fluctuations as a function of j, showing that statistical fluctuations produce less noise at higher j values.

The NN algorithm works best for small clusters when Σ_j is averaged over a few values of j in the range $3 < j < 20$ (Casertano & Hut 1985; Schmeja 2011); the lowest j values are sensitive to statistical fluctuations, while at high j values, the signal from small clusters becomes too diluted. We would need to select j values as low as 3 to probe within the cluster radius. However, after reviewing results for various ranges from $j = 3$ to $j = 12$, we find that statistical fluctuations are sufficiently damped around $j > 8$ (Figure 5).

We therefore use the range $j = 8$–12 as the basis for our cluster-finding analysis. We calculate the difference between Σ_j and the background density $\Sigma_{\rm bg}$ in units of $\sigma_{\rm bg}$ for $j = 8$–12. We then obtain the average and median differences across these j values for each target field (Figure 6). Systems with higher Σ_j above the background $\Sigma_{\rm bg}$ are more likely to be physical clusters.

We again compare our results with the random field data. Since NN is also calculated from a specific target star, we

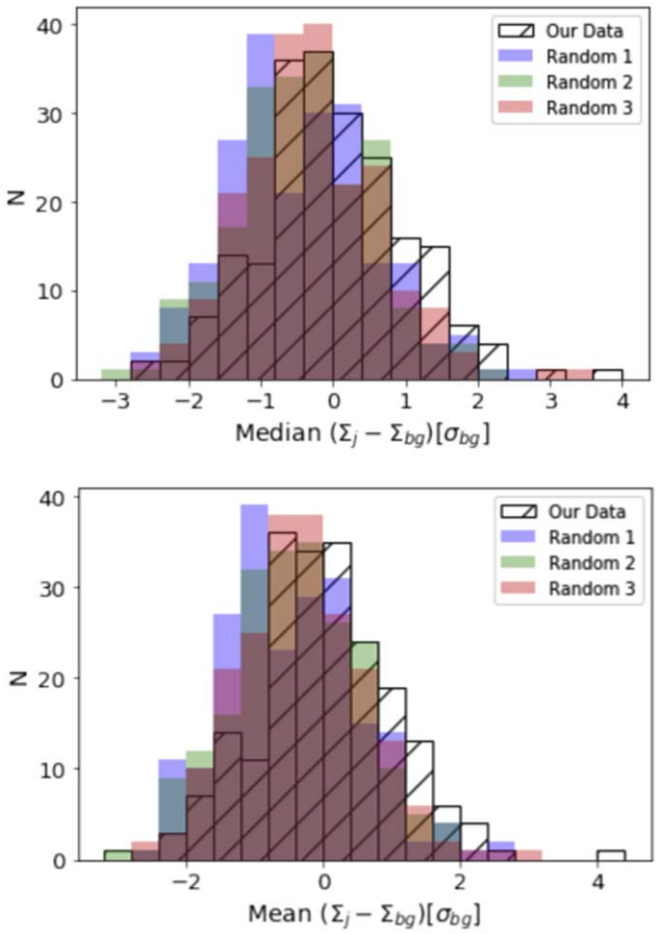

Figure 6. Our NN results for the average (bottom) and median (top) overdensities for $j = 8$–12 as well as the three random data sets. Our observed data are shown in black, while the random-field data sets are colored as shown. The Wilcoxon test indicates that our observed data and random fields are distinct, while two out of three of our Rosenbaum test results indicate the contrary.

choose the star nearest the center in the random data sets as the origin of this algorithm. These results are plotted with our NN results in Figure 6.

The density distributions peak at slightly negative values because the density measurement is centered on a star rather than a random, starless point; it is caused by the fact that positions centered on stars are necessarily farther from the nearest star than random positions between them, which causes the stellar densities to be underestimated at the lowest j values (Casertano & Hut 1985).

The Wilcoxon and Rosenbaum tests comparing the observed and random-field data are given in Table 1. The statistical tests yield ambiguous results. While the Wilcoxon test shows a significant likelihood of TIB clusters being present, the Rosenbaum test for NN, like the previous results for FOF, find that our observed data are indistinguishable from two of the three random-field data sets. These contradicting statistical test results suggest that the observations are in a regime where TIB clusters are marginally detected, which is further discussed in Section 3.

2.3. Stacked Fields

Given the nondetection, or at best marginal detection, of any clusters by the above methods, we can improve our detection sensitivity for the aggregate sample by stacking the data for all fields. We measure the stellar density as a function of radius from each target star and then take the median of all of our target fields at each radial step. We do the same for the random fields. For these, the densities are measured by centering on the star closest to the center of the field, as before. The radial density profiles for the observed data and the random data sets are shown in Figure 7. The sawtooth pattern in the unsmoothed plots results from oversampling the relatively small number of discrete stars relative to the higher resolution pixel grid: the value of the stellar density associated with individual stars decreases with radius until additional stars are included within the target area. The random-field data show a trend of increasing stellar density with radius that flattens out around 60 px. This is again the statistical effect caused by selecting a star, rather than a truly random position, as the origin for the counting algorithm.

The observed data do show an excess relative to the random fields at radii <60 px, suggesting the presence of a real aggregate enhancement that may be due to the presence of some TIB clusters. This will be discussed further in Section 5.

3. Subpopulations

3.1. Runaways and Nonrunaways

We know that a large fraction of the field OB stars are runaways, which would not be in TIB clusters. Oey et al. (2018) identified runaways with transverse velocities $>30\,\mathrm{km\,s^{-1}}$ from Gaia proper motions. Thus, we can evaluate the reliability of the cluster-finding algorithms by determining how many of the best cluster candidates are identified as runaways. For FOF, the best TIB candidates are those with the highest N_* and M-values, and for NN, they are the target fields with the highest overdensities relative to the background. We use the residual transverse velocities $v_{\mathrm{loc},\perp}$ that were measured by Oey et al. (2018) relative to the local velocity fields, adopting their runaway definition of $v_{\mathrm{loc},\perp} > 30\,\mathrm{km\,s^{-1}}$.

Of the top 20 TIB candidates from the FOF analysis, eight are runaways among the top N_* candidates, and seven are among the top M-test candidates. For the NN algorithm, nine and eight are among the top 20 candidates based on the median and average overdensities, respectively. These findings are summarized in Table 2, where these runaways are identified. Thus we see that on the order of one-half of even the top 20 TIB candidates for both FOF and NN are runaways. This is reasonably consistent with the 2/3 fraction of runaways in the RIOTS4 sample (Dorigo Jones et al. 2020). Although the Wilcoxon tests in Section 2 show a significant difference between the observed and random fields, the number of runaways among the best TIB candidates underscores the role of random density fluctuations in generating signals suggestive of TIB clusters by our algorithms.

The FOF algorithm shows significantly more runaways among the top five TIB candidates for both the N_* and M criteria than obtained by NN. Even three of the top five candidates identified by the N_* criterion are runaways. On the other hand, for both NN criteria, none of the top five candidates include known runaways. We caution that the Gaia measurement errors are relatively large ($\sim 28\,\mathrm{km\,s^{-1}}$), and there is moreover uncertainty regarding the proper motion for any individual object; since the RIOTS4 runaway threshold is $30\,\mathrm{km\,s^{-1}}$, the measurement errors leave open the possibility

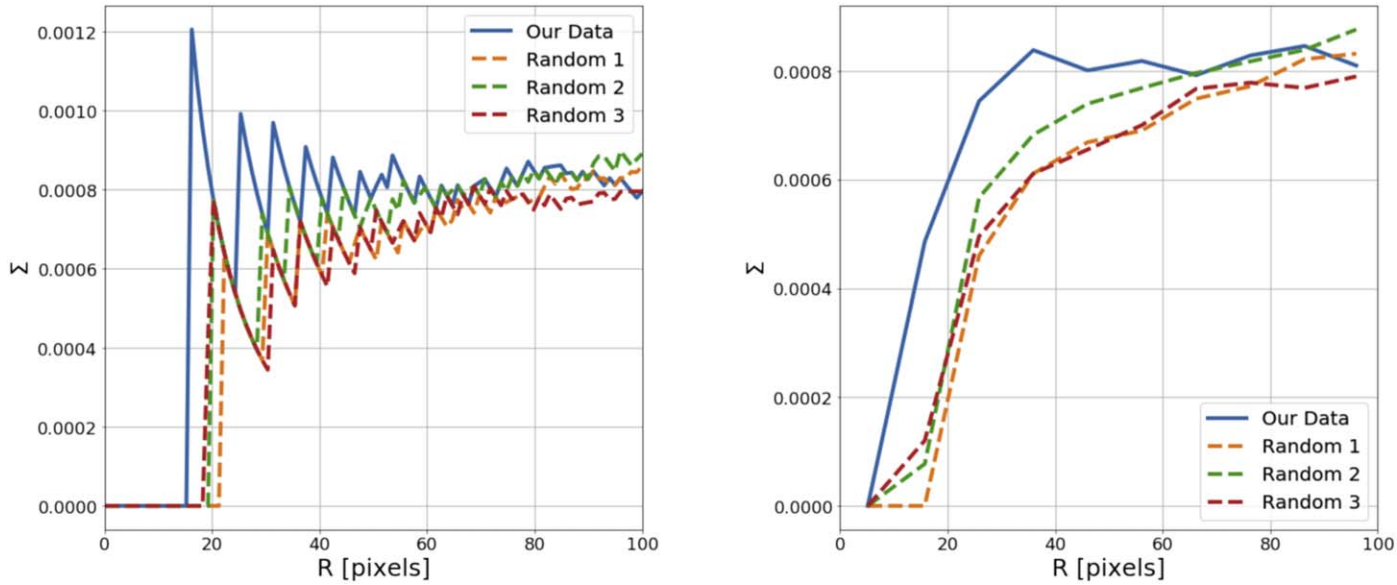

Figure 7. Comparison of stacked target fields with stacked random data sets. This plot shows the stellar density as a function of radius from the target for our observed data (solid blue), along with those for our three random data sets (dashed lines). It is binned by 1 (left) and by 10 (right). The observed data show a modest excess relative to the random fields at radii <60 px, suggesting the presence of a real aggregate enhancement. The sawtooth patterns in the unsmoothed plot are due to undersampling of the data (see text).

Table 2
Runaways among Top TIB Candidates [a]

Target[b]	FOF N_*	FOF M-value	NN Average	NN Median
3815	⋯	○	⋯	○
13896	⋯	⋯	○	○
27600	⋯	○	○	○
27712	⋯	○	⋯	⋯
27884	•	★	⋯	⋯
30492	⋯	⋯	○	○
43411	⋯	⋯	○	○
67893	○	⋯	⋯	⋯
70149	•	⋯	⋯	⋯
71409	★	○	⋯	⋯
71652	•	⋯	○	○
72208	★	○	⋯	⋯
73952	○	⋯	⋯	⋯
74946	★	★	•	•
75626	⋯	⋯	•	•
77734	⋯	⋯	•	•

Notes.
[a] Open circles, filled circles, and stars correspond to objects identified among the top 20, 10, and 5 TIB candidates, respectively.
[b] ID from Massey (2002).

that a significant fraction of nonrunaways are misidentified as runaways and could therefore be TIBs. However, note that this interpretation also depends on, and is consistent with, the difference between the FOF and NN results being due to the existence of a few real TIB clusters among the top candidates identified by NN.

Separating our sample into runaway and nonrunaway targets should strengthen the signal of any real TIBs among the latter. Thus, we compare the results of our cluster-finding algorithms for these subsamples in Figures 9–11. We also apply the Wilcoxon and Rosenbaum tests to compare the runaway and nonrunaway targets to their respective random fields, as well as to each other. Our results are shown in Table 1.

The Wilcoxon and Rosenbaum test results for the runaways are essentially identical to those for the full sample. For runaways, we would expect to not see any statistical differences from random fields. We therefore believe that the positive detections from the Wilcoxon test are not due to cluster detections, but instead result from other effects, like the possible nonrandom spatial distribution of field stars suggested earlier. This is consistent with the stacked field results for runaways, where at small radii they appear to have ambiguous, but slightly higher, densities.

Additionally, runaways show a significant fraction of targets found in lower density environments, as expected since they quickly move away from the dense cluster-forming environments where they originated. Figure 8 shows Σ_j and the corresponding background density, $\Sigma_{\rm bg}$, as a function of R_j, the mean radius of the jth nearest neighbor. The nonrunaways on average have greater Σ_j and $\Sigma_{\rm bg}$, while runaways on average have higher R_j values, indicating that runaways tend to be in target fields with lower stellar density. This is also reflected in Figure 9, wherein the peaks of the nonrunaway distributions are at larger values than those for the runaways.

For FOF, the nonrunaways do not show statistically significant differences from the runaways. They exhibit the same behavior that is seen for both the full and the runaway data sets, showing significant Wilcoxon test results but not Rosenbaum test results. For NN, however, the nonrunaways do show statistically significant differences from the runaways. In the NN density distribution comparisons with the random fields, the Wilcoxon results give p-values that are statistically significant and lower by an order of magnitude than those for the runaways. However, the Rosenbaum results are more ambiguous because only two NN comparisons with random fields show a statistically significant difference. This again demonstrates that the frequency of any TIB clusters in the observed data set is on the order of the random noise in our fields.

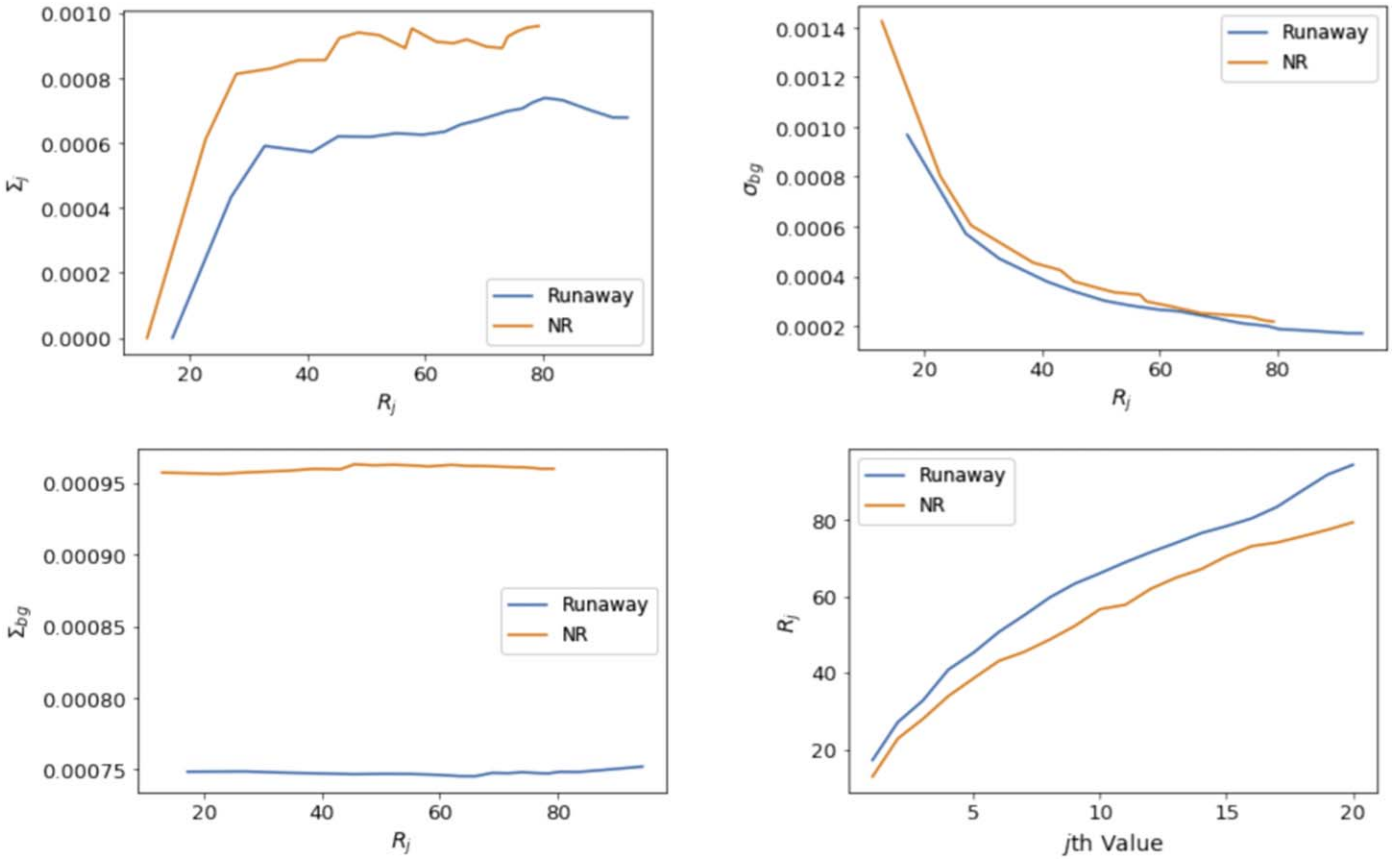

Figure 8. Distribution of various NN values for our runaway and nonrunaway (NR) data sets: the median Σ_j (upper left), median $\sigma_{\rm bg}$ (upper right), and median $\Sigma_{\rm bg}$ (lower left) as a function of median R_j values. The lower right plot is of the median R_j values as a function of j. On average, the runaway data set shows higher values for R_j, but lower Σ_j and $\Sigma_{\rm bg}$ values, than the nonrunaways, indicating that they are found in lower density environments.

When compared to each other, the runaway and nonrunaway distributions also look noticeably different (Figure 9 and 10), confirming these trends. Since the runaway and nonrunaway data sets are independent of each other, we are able to use the Kolmogorov–Smirnov (K-S) test and also the Anderson–Darling (A-D) test when comparing these distributions. This version of the K-S test gives more weight to the tails of the distributions, which in our case are more sensitive to the detection of TIBs. The resulting p-values of the A-D and K-S tests are also shown in Table 1. For FOF, we have statistical test results similar to NN between the runaway and nonrunaway distributions of N_* and M-values (Figure 10); however, their A-D and K-S tests are unable to distinguish the runaways and nonrunaway distributions from each other, although we are able to see that nonrunaways are skewed toward higher values.

Meanwhile, the NN data (Figure 9) do show evidence that the runaway and nonrunaway density distributions are different, with p-values of 0.022 and 0.035 in the K-S test, while the A-D results are close to the critical range, between $p = 0.05$ and 1.0. In Figure 9, runaways peak at lower values than the nonrunaways, and their maximum overdensities are less than those of the random-field data sets. On the other hand, nonrunaways have both higher peak and maximum values that are distinct from the random-field data.

Our stacked fields also show differences between our runaway and nonrunaway data sets (Figure 11). We find that the runaways show less variation from the random-field data sets, although they do appear to show, with some ambiguity, a significant density enhancement at the lowest radii that may be a product of the systematic errors similar to those found in NN. In contrast, the nonrunaways clearly show higher, and more centrally concentrated, densities than the nonrunaways. In Figure 11, we can see that these higher densities are present even when smoothing our distribution of observed overdensities. These higher densities may be due to the presence of TIB clusters and are likely the cause of the aggregate enhancement seen in Section 2.3. This is further discussed in Section 5.

In summary, any signal of TIBs in our sample should be strengthened in nonrunaway data sets, while we expect runaway fields to behave more like random fields. Despite its positive detections, the FOF algorithm is not sensitive to the differences between nonrunaway and runaway fields. Therefore, its results are not a reliable indicator of the presence of TIBs in our sample and cannot be used to estimate the number of TIB clusters. On the other hand, the results given by NN and the stacked fields do show significant differences between the runaways and nonrunaways, which are consistent with the presence of a small, but real, number of TIB clusters. This is supported by the statistical differences between nonrunaway and runaway distributions given by their respective K-S and A-D test results. The relative effectiveness of NN and FOF is consistent with the analysis by Schmeja (2011), who find that NN is a superior cluster-finding algorithm when compared to

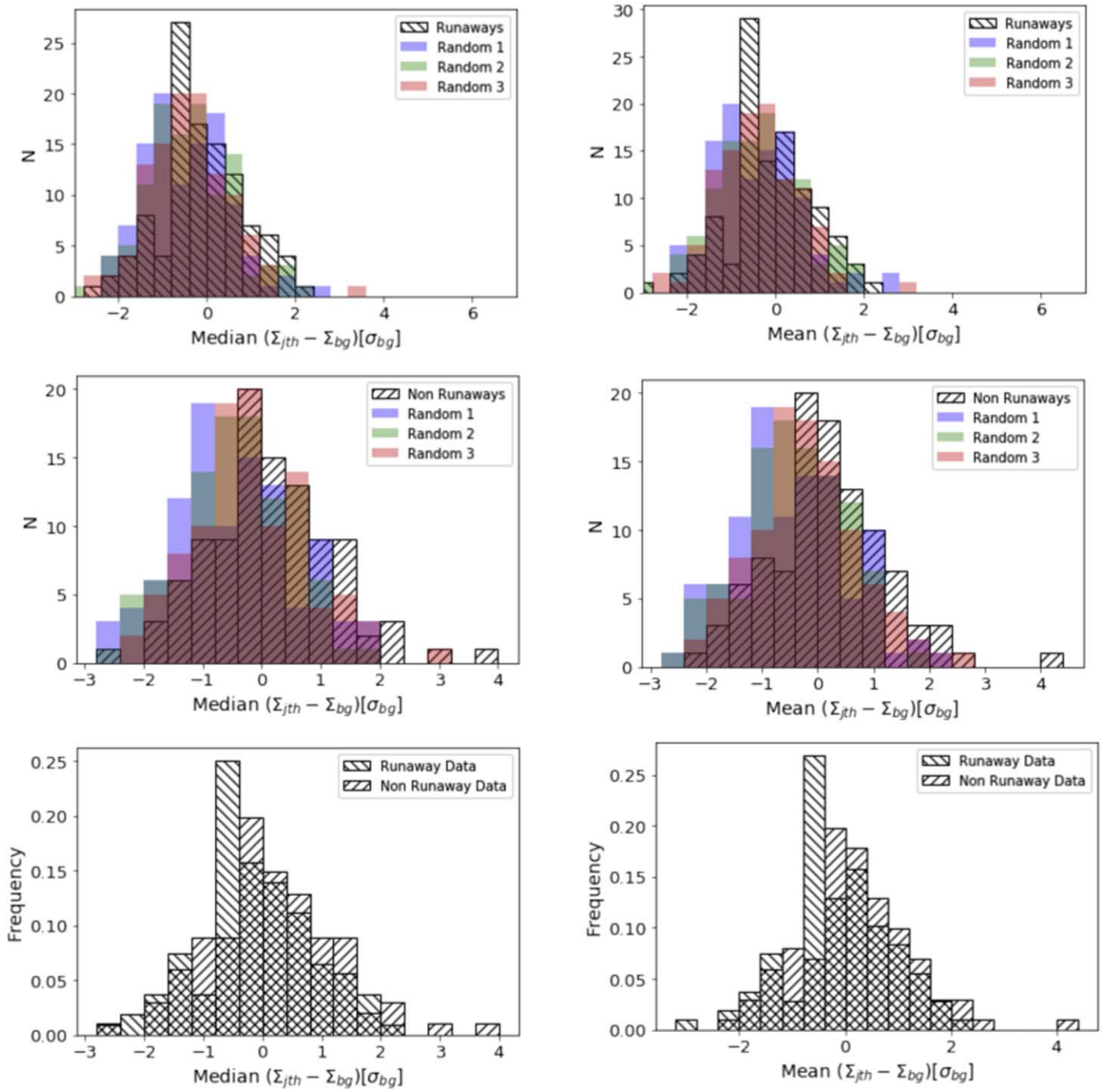

Figure 9. NN density distributions comparing our observed data for runaway (top) and nonrunaway targets (middle) with their respective fields in the random data sets. The observed data are shown in black, while the three random data sets are colored as shown. The left column shows the median overdensities for $j = 8$–12, and the right column shows the averages. The bottom row compares the runaway (stars) and nonrunaway (lines) distributions normalized with respect to their total number. The Rosenbaum and Wilcoxon tests give contradicting results on whether our runaway targets are distinct from a random distribution. However, for nonrunaway targets, these tests show strong statistical differences from a random distribution. The nonrunaway and runaway distributions are also statistically different from each other in their Kolmogorov–Smirnov test.

other methods, including the minimum spanning tree, on which FOF is based.

3.2. In Situ Field OB Stars

Conversely to runaways, we can also examine objects that have been identified as field OB stars that formed in situ. Oey et al. (2013) identified 14 strong candidates in the RIOTS4 survey, based on their dense, symmetric H II regions and radial velocities consistent with local H I systemic velocities. Of these, 10 are in our data set. We might expect that a few of these should be runaways, and we might expect some to be among the best TIB candidates from our cluster-finding algorithms.

We find that only two of the in situ targets ([M2002] SMC-70149, 71409) are among the top 20 FOF TIB candidates, and another two of them ([M2002] SMC-69598, 75984) are among the top NN candidates. Instead, five of the in situ candidates, including

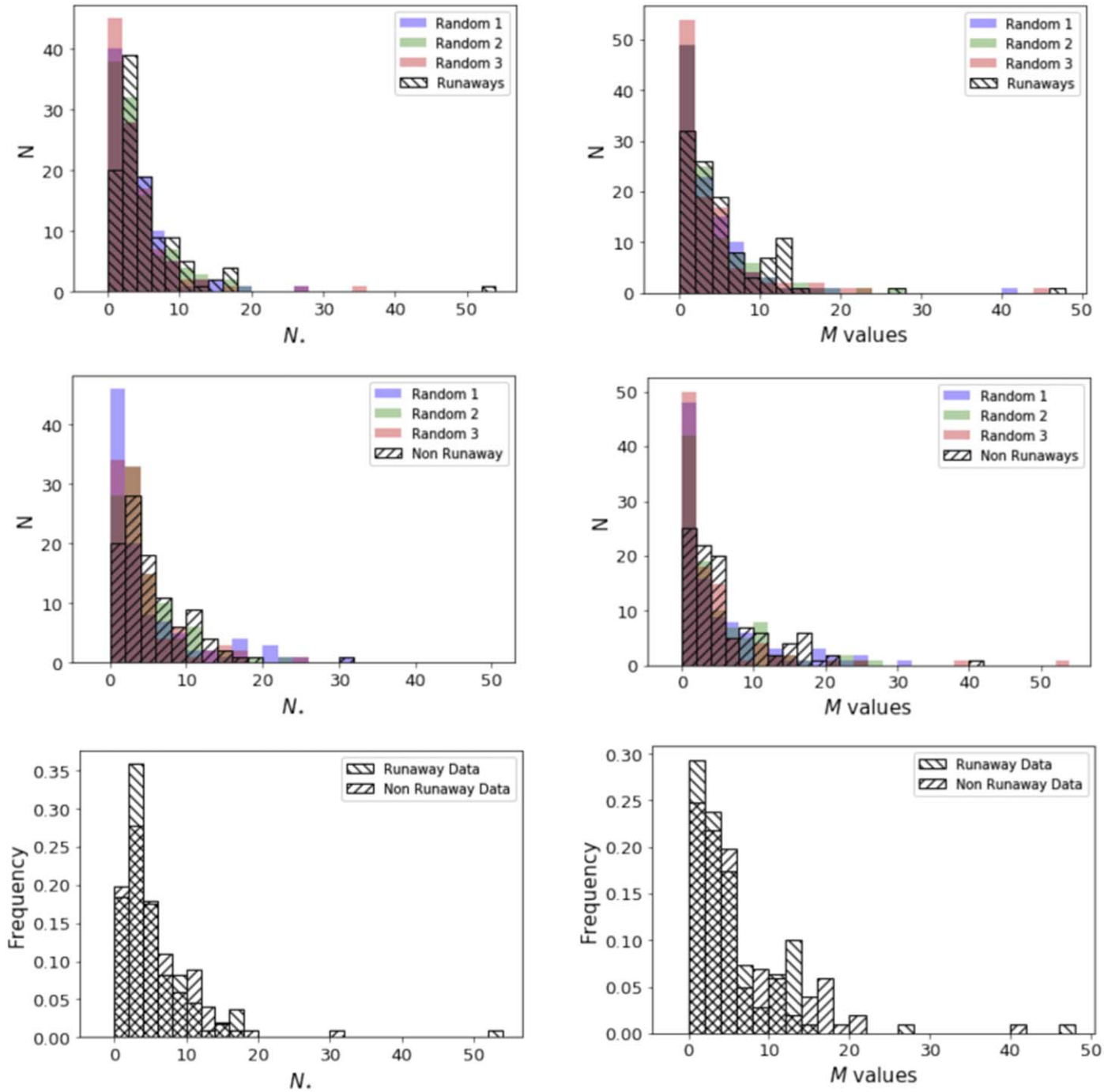

Figure 10. FOF results comparing our observed data for runaway (top) and nonrunaway targets (middle) with their respective fields in the random data set. The bottom row compares the runaway and nonrunaway distributions normalized with respect to their total number. The left column shows the N_* distribution, while the right column shows the M-value distribution. Our observed data are in black, while the random data set is in blue. In the bottom row, nonrunaway and runaway normalized distributions are shown with different hatching as shown. The Wilcoxon test identifies the runaway and nonrunaway distributions as distinct from random distributions, but the Rosenbaum does not. The A-D and K-S tests are unable to distinguish the runaway and nonrunaway distributions from each other.

two in the top 20 for FOF, are identified as runaways. Images of these runaway-star fields are shown in Figure 12, and their kinematic information (Oey et al. 2018)[8] is shown in Table 3. Two of these have low runaway velocities (targets [M2002] SMC-35491 and 71409) and are also consistent with being nonrunaways within the errors. However, others have velocities far above the runaway threshold of $v_{\mathrm{loc},\perp} > 30\ \mathrm{km\ s^{-1}}$ (targets [M2002] SMC-36514, 67334, and 70149).

The runaway frequency in this subsample is larger than what we find in Section 3.1. This is likely because the in situ candidate sample was selected to have no visual evidence of TIBs, and therefore these objects are more likely to be either runaways or candidates for isolated in situ star formation. Since we know the fraction of runaways in our sample is high (Oey et al. 2018; Dorigo Jones et al. 2020), this further enhances the

[8] In Table 1 of Oey et al. (2018), columns 11 and 13 correspond to the systemic R.A. and decl. velocities, respectively, of the local fields for each target star.

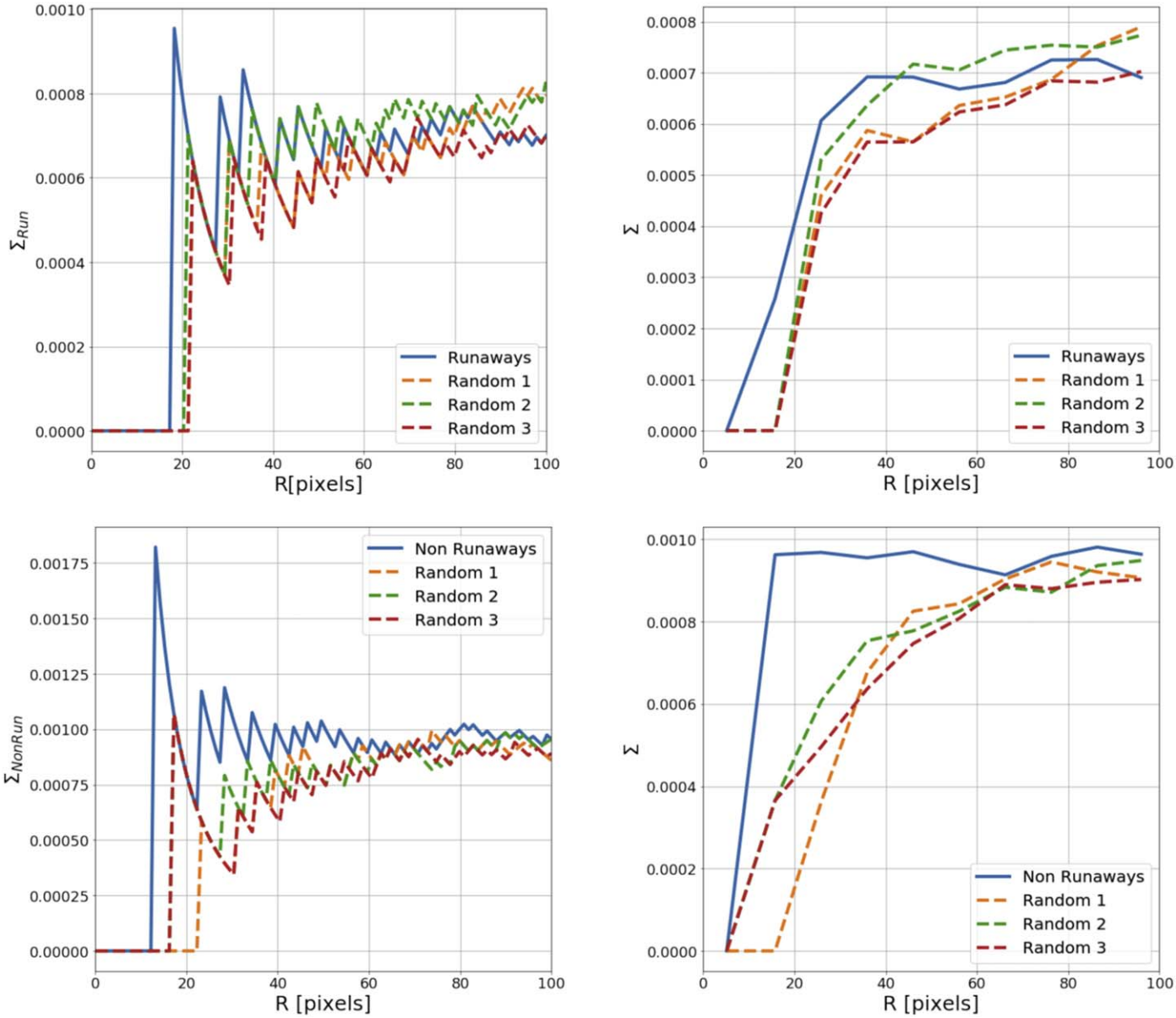

Figure 11. Plots of observed overdensities to those for random fields, as a function of radius, for our runaway targets (top) and nonrunaway targets (bottom). They are binned by 1 (left) and by 10 (right). Our runaway targets appear to have ambiguously higher densities at very small radii that are not due to real density enhancements. However, nonrunaway targets do show centrally concentrated densities.

likelihood that objects selected to appear isolated are runaways. Indeed, the fact that only half of the objects are confirmed runaways implies that the rest remain candidates for highly isolated, in situ star formation. Such objects would not be runaways or walkaways, nor would they show TIBs. For example, the H II regions of targets [M2002] SMC-66415 and 69598 show "elephant trunks" pointing toward the targets, as shown in Figure 1 from Oey et al. (2013), which are difficult to explain if the objects originated far away.

4. Fraction of TIB Clusters in the SMC

The nonrunaway sample shows slightly positive skews in the NN stellar density distributions. These are statistically significant and, as argued above, consistent with the possible presence of TIB clusters. If there are any real clusters in our sample, we can estimate their potential number by determining the excess induced by the positive skew of the observed distributions relative to those of the random data. We obtain the excess number of target fields having values beyond the midpoints between the medians of our observed data and the random data set. Table 4 summarizes our estimates for the percentage of TIB clusters identified in our full sample and subsamples. These estimates assume Poisson errors and do not include any systematic effects.

When estimating their frequencies, we obtain relatively large values in both runaway and nonrunaway distributions, as shown in Table 4. For the runaways, we do not believe that this excess corresponds to true cluster detections, since our targets were selected to be far from any OB association and runaways are unlikely to originate as TIBs, and instead we believe that these are caused by systematic effects. These could, for example, be due to the background stars having positions that are not purely random. As noted above, Figure 9 shows that the

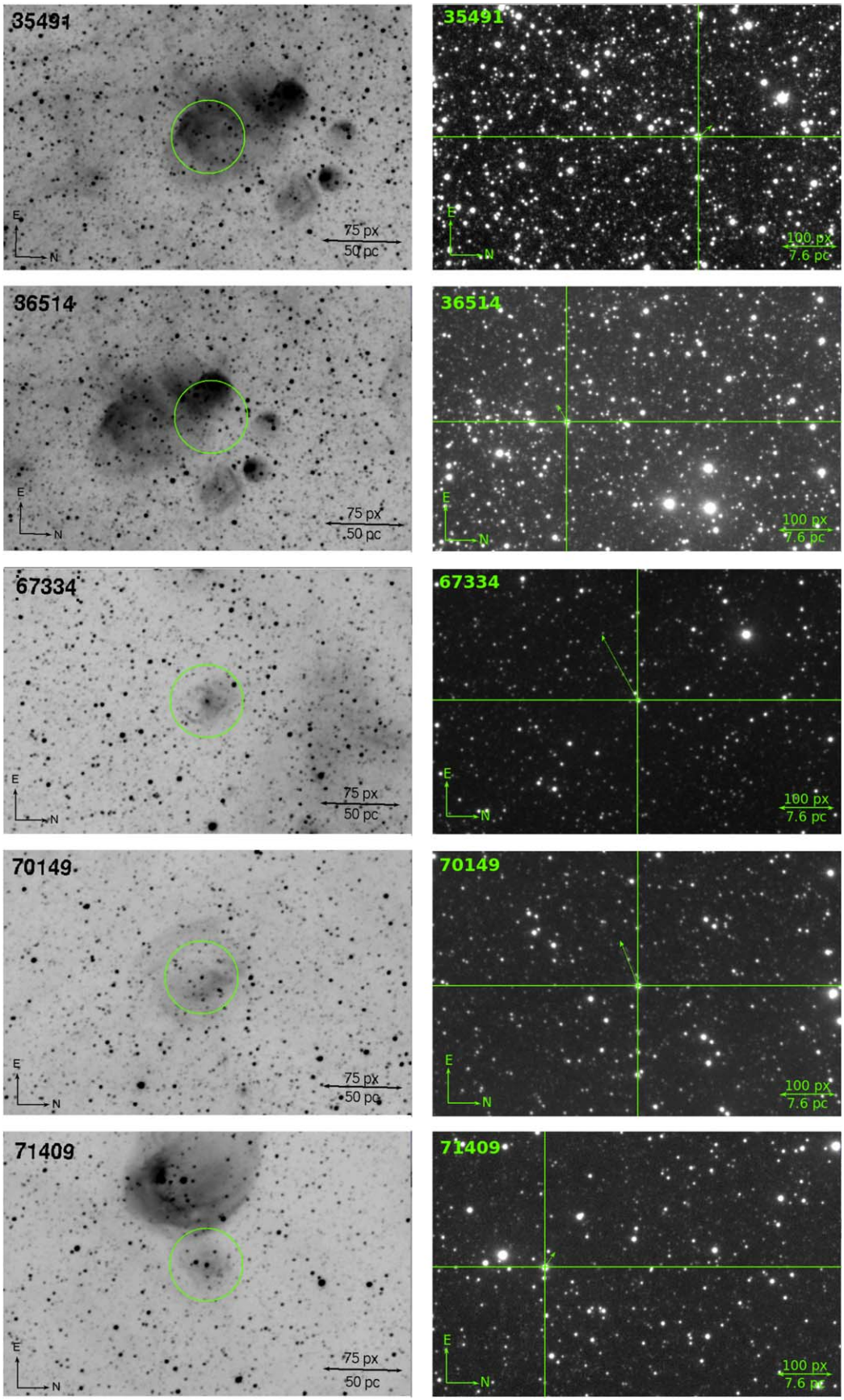

Figure 12. Five in situ candidates that were classified as runaways in our own study. North is to the right and east is up. On the left side are the Hα images, and on the right are the *I*-band images. In the Hα images, the target is highlighted by the circle. On the right, the green arrow shows the target's $v_{\mathrm{loc},\perp}$ (Table 3). Their kinematic data are shown in Table 3.

Table 3
Kinematic Data for Isolated In Situ Candidates Identified as Runaways

Target[a]	R.A. Velocity[b] (km s^{-1})	Error (km s^{-1})	Decl. Velocity[b] (km s^{-1})	Error (km s^{-1})	$v_{\mathrm{loc},\perp}$[c] (km s^{-1})	Error (km s^{-1})	Radial Velocity[d] (km s^{-1})	3D Velocity[e] (km s^{-1})	Error (km s^{-1})
35491	22	20	25	19	34	27	−23	40	29
36514	90	29	−51	24	103	38	−8	104	39
67334	119	24	−66	20	136	32	54	146	33
70149	82	29	−32	25	88	39	1	88	40
71409	28	26	19	15	33	31	…	…	…

Notes.
[a] ID from Massey (2002).
[b] The R.A. and decl. velocities are relative to local systemic velocity and are calculated using the R.A. and decl. velocities from Oey et al. (2018).
[c] Residual transverse velocities from Oey et al. (2018).
[d] From Lamb et al. (2016). The error in RV is on average 10 km s^{-1}.
[e] Space velocity relative to local frame.

Table 4
Estimated Percentage of TIB Clusters[a]

	Full Sample %	Nonrunaways %	Runaways %	Full Data Subtracted[b]	Nonrunaways Subtracted[b]
NN Average vs. Random 1	15 ± 2.9	22 ± 5.1	11 ± 3.4	4 ± 4.5	11 ± 6.1
NN Average vs. Random 2	12 ± 2.6	21 ± 5.0	8.3 ± 2.9	3.7 ± 3.9	1 3± 5.8
NN Average vs. Random 3	12 ± 2.6	18 ± 4.6	8.3 ± 2.9	3.7 ± 3.9	9.7 ± 5.4
NN Median vs. Random 1	17 ± 3.1	23 ± 5.3	13 ± 3.7	4.0 ± 4.8	10 ± 6.5
NN Median vs. Random 2	15 ± 2.9	22 ± 5.1	12 ± 3.5	3.0 ± 4.5	10 ± 6.2
NN Median vs. Random 3	11 ± 2.4	16 ± 4.3	10 ± 3.2	1.0 ± 4.0	6.0 ± 5.4

Notes.
[a] "NN Average" or "Median" specifies the method of combining the NN stellar density calculations for $j = 8$–12. "Random 1," "Random 2," and "Random 3" refer to the respective random-field data sets.
[b] Columns 5 and 6 show the estimated frequencies obtained by subtracting the runaway frequencies from those of the full sample and nonrunaway samples, respectively.

runaway density distribution matches those of the random fields. Instead, the positive runaway detections likely originate from objects that have moved into the line of sight toward a density enhancement.

As shown earlier, half of the top 20 potential cluster candidates from NN were actually runaways (Table 2), showing that it is possible for runaways to appear to be in TIB clusters just by happenstance. We take the percentage of positive detections for runaways to be the percentage of TIBs that arise by chance. To obtain an estimate for the TIB cluster frequency, we therefore subtract this frequency of false positives from the raw estimates from the nonrunaways and the full sample. The final resulting estimates are also shown in Table 4, which support the existence of a low fraction of TIBs in our sample.

In general, the final, corrected TIB frequency estimates in Table 4 for nonrunaways are 2–3 times that for the full sample. This is consistent with the bulk of these estimates representing real clusters, since nonrunaways are about half the sample (101 out of 210 targets).

We show the top 10 cluster candidates identified by NN in Table 5 and their images in Figure 13. A few of these candidates visually appear to be in clusters. However, the rest of them have ambiguous status, again consistent with the scenario that the TIB cluster frequency is small and of marginal statistical significance. Among the top 10 candidates identified by both NN algorithms, four are not included in the top 20 FOF candidates. Interestingly, three of these objects, [M2002] SMC-81646, 75984, and 69598, are in less dense fields (Figure 13).

We note in Figure 13 that some of our field OB stars have companions associated by NN that appear brighter than our targets in the *I*-band. A few of these red and yellow stars may be evolved massive stars, implying that our target OB star may not always be strongly isolated from other high-mass stars, since our selection criteria are based only on separation from luminous blue stars (Lamb et al. 2016). For example, in at least one case, [M2002] SMC-81646, the bright companion is a likely SMC red supergiant, based on its radial velocity (Massey 2002; Massey & Olsen 2003). Another object, [M2002] SMC-58947, has a possible yellow supergiant companion ($B - V = 0.65$; Massey 2002), but this could also be a foreground G star at a distance of 380 pc, which places it 270 pc below the Galactic plane ($b = -44\overset{\circ}{.}7$). The other two cases in Figure 13, [M2002] SMC-6908 and 46241, show candidate SMC AGB and RGB stars, respectively (Boyer et al. 2011), which are therefore likely field stars in the line of sight. These stars are much less luminous in *B* and *V* than our targets. But in general, we caution that occasional evolved supergiants may be present near other target stars in our sample.

With the estimates from our nonrunaway data in Table 4, we can set an upper limit on the frequency of TIB clusters in our sample. For the nonrunaways, the average excess over the random fields is 11% ± 3.3%, combining the values based on the average results for $j = 8$–12, corrected for the false-positive

Table 5
Top 10 Candidates from NN for Nonrunaway Targets[a]

Target[b]	NN Median		NN Average		FOF N_*		FOF M-value	
	Value	Rank	Value	Rank	Value	Rank	Value	Rank
47459	4.0	★	4.0	★	19	★	25	★
6908	2.9	★	2.6	★	11	•	17	•
81646	2.2	★	2.3	★	5	⋯	2.5	⋯
46241	2.2	★	2.2	★	14	★	16	•
75984	2.2	★	2.2	★	8	⋯	5.2	⋯
58947	1.9	•	1.8	•	16	★	20	★
25639	1.8	•	1.8	•	11	•	16	•
42260	1.5	•	1.6	•	3	⋯	4.0	⋯
69598	1.5	•	1.6	•	12	•	8.2	⋯
24213	1.5	•	1.5	∘	6	⋯	11.2	∘
13774	1.3	∘	1.5	•	12	•	21	★

Notes.
[a] Open circles, filled circles, and stars correspond to objects identified among the top 20, 10, and 5 TIB candidates, respectively. There are 11 candidates because the median and average results share the same top 10 with one exception.
[b] ID from Massey (2002).

rate, while for the excess based on the median calculations, the average TIB cluster frequency is 8.7% ± 3.5%. Overall, we can use these estimates as an upper limit to the frequency of TIB clusters in the entire field sample, which is on the order of ∼4%–5% since nonrunaways represent about half of the full sample.

Although Figure 13 and Table 4 show few clear examples of TIBs, our results suggest that our estimated 4%–5% fraction of TIB clusters might be real. On the one hand, statistical tests indicate a lack of positive detections for TIB clusters. There are mixed results for NN, with positive results from Wilcoxon but at least one negative result from the Rosenbaum test for all three data sets. These results seem to indicate a lack of evidence for TIBs within our sample. But on the other hand, there is a contrast between our runaway and nonrunaway populations that is consistent with expectations if TIB clusters are present. The positive skews lead to estimated TIB cluster fractions for nonrunaways from all the algorithms that are roughly double the value for the full data set, consistent with TIB clusters being associated with nonrunaways, as expected. We also see that the nonrunaways show a statistically significant distinction from the runaway NN density distributions using the K-S test and p-values below 0.1 for the A-D test. Furthermore, the stacked fields show clear, centrally concentrated densities only for the nonrunaways. Thus, although the statistical results are quantitatively inconclusive, the evidence does support a TIB cluster frequency of up to 4% or 5%.

5. Discussion

Our results show that in situ star formation is rare at best, with at most 4%–5% of our target field OB stars being in small TIB clusters. This result is consistent with the work of Dorigo Jones et al. (2020), who use stellar kinematics to determine that runaways and walkaways comprise the overwhelming majority of our sample.

Furthermore, the fact that five out of the 14 candidates for in situ field OB stars found by Oey et al. (2013) turn out to be runaways (Section 1.1) suggests that their criteria for identifying in situ field OB stars are surprisingly ineffective, therefore casting some doubt on the remaining nine candidates in their sample. This result is consistent with Gvaramadze et al. (2012), who determined that many isolated in situ candidates are actually runaways. Moreover, for the other five of the in situ candidates that are in our sample, three are not among our top cluster candidates, suggesting that they are not TIB stars. This, however, does not rule out the possibility that they are actually rare cases of isolated field OB star formation and that the five runaways may be a product of the selection bias within the sample.

There are two possible explanations for the apparent lack of TIB clusters: either they could be evaporating on very short timescales, or they simply do not form. Oey et al. (2004) found that the cluster mass function is fully consistent with the existence of TIBs, which would represent the lowest-mass clusters containing single O stars. Indeed, TIBs could comprise up to ∼50% of field OB stars for the observed cluster mass function (Lamb et al. 2016). Our results may be consistent with the smallest clusters undergoing infant mortality, and therefore causing their OB stars to appear isolated. de Grijs & Goodwin (2008) show that a large fraction of clusters in the SMC evaporate on 3–10 Myr timescales. Therefore, the presence of small, unbound associations with OB stars would not be unlikely, as also suggested by Ward et al. (2020).

On the other hand, the smallest clusters that form OB stars may have masses larger than those probed by our sample selection criteria. Lamb et al. (2010) estimated a lower limit of ∼20 $M_\odot$ for the cluster mass function, based on observations and Monte Carlo simulations that assumed power laws for both the cluster and stellar mass functions. If the cluster lower-mass limit has a larger value, then this could be an effect of the low metallicity environment in the SMC, which could inhibit the formation of the smallest clusters.

Alternatively, since we find that few, or none, of our targets correspond to small clusters stochastically forming OB stars, then this may support the $m_{\rm max} \propto M_{\rm cl}^{2/3}$ relation from Bonnell et al. (2004). In this scenario, the smallest clusters do exist, but they never form OB stars. Stellar mergers have been proposed to explain observed exceptions (Oh & Kroupa 2018), perhaps including the estimated fractions in Section 4.

Since the core-collapse model for massive star formation does allow the occasional formation of OB stars as TIBs, the

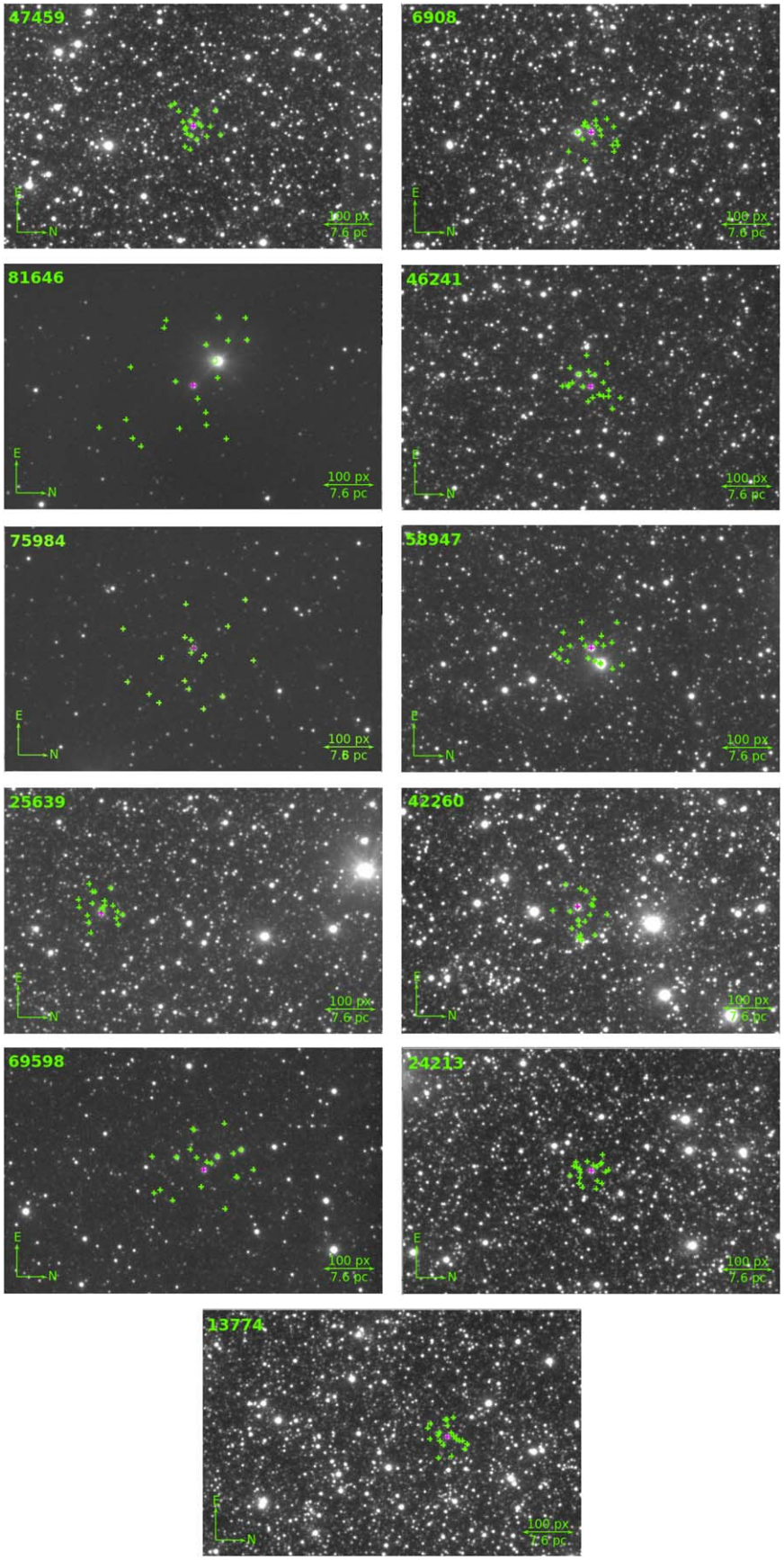

Figure 13. Top 10 cluster candidates from NN for the nonrunaways in our study. Eleven candidates are shown because the median and average $j = 8$–12 results share the same top 10 targets, except for one. North is to the right and east is up. Here 100 px corresponds to 26″ in angular scale. Each target is shown in magenta with its 20 jth nearest neighbors in green. Their top 20 ranking in each of our criteria are shown in Table 5.

observed lack of TIB clusters may favor the competitive accretion model. However, it may be that our nonrunaway field OB sample is not large enough to distinguish between these models, and, as discussed in Section 4, relatively isolated star formation could still occur in very rare situations. Our results remain consistent with the estimate of de Wit et al. (2004), who found that 4% ± 2% of their sample cannot be traced to formation in a cluster/OB association, suggesting that these could be either TIBs or candidates for isolated in situ star formation. Additionally, our results are also consistent with OB stars forming in small, unbound associations, which would support the formation of massive stars by monolithic cloud collapse (Ward et al. 2020). The small fraction of TIB clusters in our observed data set would occur if these associations disperse quickly, thereby leaving apparently isolated OB stars. In any case, our new limits on the existence of TIBs set much more stringent constraints on the formation of massive stars in relative isolation.

6. Conclusion

In summary, we use two cluster-finding algorithms, friends of friends and nearest neighbors, to determine whether our field OB stars are the "tips of icebergs" on tiny clusters based on stars having $I < 19.0$. Our 210 target stars are a subset of the statistically complete RIOTS4 survey of field OB stars in the SMC (Lamb et al. 2016) that are also included in the *I*-band imaging from the OGLE-III survey (Udalski et al. 2008). We compare our observed data to three realizations of random-field data sets for each field. We also measure the stellar density as a function of radius from the targets in the stacked fields to search for a signal of TIB clusters in our sample.

Our results show that there are very few TIBs in our sample, but that a small number likely do exist. Results for both cluster-finding algorithms show strong statistical similarities in the spatial distribution of our observed data and random-field data sets. Indeed, the FOF algorithm, which we confirm to be less effective than NN (Schmeja 2011), is unable to statistically identify a difference between runaway and nonrunaway subsamples, highlighting the low occurrence of TIB clusters.

However, the NN algorithm and the stacked fields analysis do show significant differences between the runaways and nonrunaways, suggesting the presence of a small number of TIB clusters. The 101 nonrunaway stars show higher stellar density environments, consistent with the expectation that any TIB OB stars cannot be runaways. The stacked fields also show an excess density relative to the random fields at radii <60 px (4.6 pc). In general, the estimated fraction of TIB clusters for nonrunaway fields is 2–3 times the estimated frequency in the full sample, which is again consistent with real clusters being present, since nonrunaways make up roughly half of our full sample. Overall, our results show that ∼4%–5% of the field OB stars in the SMC are members of small clusters, and thus almost all are runaways and walkaways.

The low detection rate of TIB clusters implies that either such clusters evaporate on very short timescales, or they form rarely or not at all. This may imply that the cluster lower-mass limit is higher than that probed in our sample selection criteria. If so, these results would be consistent with the $m_{\rm max} \propto M_{\rm cl}^{2/3}$ relation (Bonnell et al. 2004), which would support the competitive accretion model of massive star formation. However, our sample may not be large enough to rule out the alternative, core-collapse model.

On the other hand, we note that our findings do support a frequency of ∼4%–5% for the presence of TIB clusters, and moreover, we cannot definitively rule out the possibility that some OB stars may form in highly isolated conditions, which would not be identified as TIBs. Although our findings cast doubt on many such candidates identified in our earlier work (Oey et al. 2013), a few still remain as compelling possible candidates of isolated OB star formation. However, it may be expected that these occur with even lower frequencies than TIB clusters. Thus, our results set strong constraints on the formation of massive stars in relative isolation.

We are grateful to Johnny Dorigo Jones and Matt Dallas for providing data related to the RIOTS4 survey. We thank our anonymous referee for insightful comments and suggestions. This research was supported by the National Science Foundation, grant AST-1514838 to M.S.O., and by the University of Michigan. M.S.O. also gratefully acknowledges hospitality from the University of Arizona that enhanced this work.

Facilities: Magellan:Baade, Magellan:Clay, OGLE.

ORCID iDs

Irene Vargas-Salazar https://orcid.org/0000-0001-7046-6517
M. S. Oey https://orcid.org/0000-0002-5808-1320
N. Castro https://orcid.org/0000-0003-0521-473X
Kaitlin M. Kratter https://orcid.org/0000-0001-5253-1338
Timothy A. Faerber https://orcid.org/0000-0002-8784-8199

References

Battinelli, P. 1991, A&A, 244, 69
Blaauw, A. 1961, BAN, 15, 265
Bonnell, I. A., Bate, M. R., Clarke, C. J., & Pringle, J. E. 2001, MNRAS, 323, 785
Bonnell, I. A., Vine, S. G., & Bate, M. R. 2004, MNRAS, 349, 735
Boyer, M. L., Srinivasan, S., van Loon, J. T., et al. 2011, AJ, 142, 103
Bressert, E., Bastian, N., Evans, C. J., et al. 2012, A&A, 542, A49
Campana, R., Massaro, E., Gasparrini, D., Cutini, S., & Tramacere, A. 2008, MNRAS, 383, 1166
Casertano, S., & Hut, P. 1985, ApJ, 298, 80
de Grijs, R., & Goodwin, S. P. 2008, MNRAS, 383, 1000
de Wit, W. J., Testi, L., Palla, F., Vanzi, L., & Zinnecker, H. 2004, A&A, 425, 937
de Wit, W. J., Testi, L., Palla, F., & Zinnecker, H. 2005, A&A, 437, 247
Dorigo Jones, J., Oey, M. S., & Paggeot, K. 2020, ApJ, 903, 43
Elmegreen, B. G. 1985, in Birth and Evolution of Massive Stars and Stellar Groups, ed. W. Boland & H. van Woerden (Dordrecht: Reidel), 227
Farias, J. P., Fellhauer, M., Smith, R., Domínguez, R., & Dabringhausen, J. 2018, MNRAS, 476, 5341
Gies, D. R. 1987, ApJS, 64, 545
Gies, D. R., & Bolton, C. T. 1986, ApJS, 61, 419
Goodwin, S. P., & Bastian, N. 2006, MNRAS, 373, 752
Griffiths, D. W., Goodwin, S. P., & Caballero-Nieves, S. M. 2018, MNRAS, 476, 2493
Gvaramadze, V. V., Weidner, C., Kroupa, P., & Pflamm-Altenburg, J. 2012, MNRAS, 424, 3037
Harries, T. J., Hilditch, R. W., & Howarth, I. D. 2003, MNRAS, 339, 157
Krumholz, M. R., Klein, R. I., McKee, C. F., Offner, S. S. R., & Cunningham, A. J. 2009, Sci, 323, 754
Krumholz, M. R., & McKee, C. F. 2008, Natur, 451, 1082
Lada, C. J., & Lada, E. A. 2003, ARA&A, 41, 57
Lamb, J. B., Oey, M. S., Segura-Cox, D. M., et al. 2016, ApJ, 817, 113
Lamb, J. B., Oey, M. S., Werk, J. K., & Ingleby, L. D. 2010, ApJ, 725, 1886
Leonard, P. J. T., & Duncan, M. J. 1990, AJ, 99, 608
Li, Y., Klessen, R. S., & mac Low, M.-M. 2003, ApJ, 592, 975
Mason, B. D., Hartkopf, W. I., Gies, D. R., Henry, T. J., & Helsel, J. W. 2009, AJ, 137, 3358

Massey, P. 2002, ApJS, 141, 81
Massey, P., & Olsen, K. A. G. 2003, AJ, 126, 2867
Oey, M. S., & Clarke, C. J. 1998, AJ, 115, 1543
Oey, M. S., Dorigo Jones, J., Castro, N., et al. 2018, ApJL, 867, L8
Oey, M. S., King, N. L., & Parker, J. W. 2004, AJ, 127, 1632
Oey, M. S., Lamb, J. B., Kushner, C. T., Pellegrini, E. W., & Graus, A. S. 2013, ApJ, 768, 66
Oey, M. S., Parker, J. S., Mikles, V. J., & Zhang, X. 2003, AJ, 126, 2317
Oh, S., & Kroupa, P. 2018, MNRAS, 481, 153
Oskinova, L. M., Steinke, M., Hamann, W. R., et al. 2013, MNRAS, 436, 3357
Parker, R. J., & Goodwin, S. P. 2007, MNRAS, 380, 1271
Poveda, A., Ruiz, J., & Allen, C. 1967, BOTT, 4, 86
Renzo, M., Zapartas, E., de Mink, S. E., et al. 2019, A&A, 624, A66
Roberts, M. S. 1957, PASP, 69, 59
Rosenbaum, S. 1965, J. Am. Stat. Assoc., 60, 1118
Schmeja, S. 2011, AN, 332, 172
Selier, R., Heydari-Malayeri, M., & Gouliermis, D. A. 2011, A&A, 529, A40
Shu, F. H., Adams, F. C., & Lizano, S. 1987, ARA&A, 25, 23
Stone, R. C. 1981, AJ, 86, 544
Udalski, A., Soszynski, I., Szymanski, M. K., et al. 2008, AcA, 58, 89
Ward, J. L., Kruijssen, J. M. D., & Rix, H.-W. 2020, MNRAS, 495, 663
Weidner, C., & Kroupa, P. 2006, MNRAS, 365, 1333
Zinnecker, H. 1982, NYASA, 395, 226
Zinnecker, H., & Yorke, H. W. 2007, ARA&A, 45, 481